

Multiscale modeling and nonlinear model predictive control for flue gas desulfurization



Vibhav Dabadghao^a, Lorenz T. Biegler^{a,*}, Debangsu Bhattacharyya^b

^a Carnegie Mellon University, 5000 Forbes Avenue, Pittsburgh, PA 15213, USA

^b West Virginia University, 1306 Evansdale Drive, PO Box 6102, Morgantown, WV 26506, USA

HIGHLIGHTS

- Detailed multi-scale dynamic model developed for Wet Flue Gas Desulfurization (WFGD).
- Index reduction applied to high-index droplet model to realize a well-posed index-1 DAE.
- Dynamic optimization formulation developed to minimize pumping costs and satisfy SO₂ recovery specifications.
- Extended to nonlinear model predictive control and demonstrated with fluctuating flue gas inputs.

ARTICLE INFO

Article history:

Received 13 July 2021

Received in revised form 10 January 2022

Accepted 18 January 2022

Available online 10 February 2022

Keywords:

Flue gas desulfurization

Index reduction

Nonlinear model predictive control

ABSTRACT

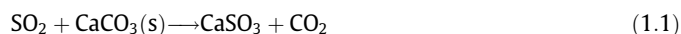
The primary source of sulfur dioxide (SO₂) emissions is flue gas from fossil fuels-based power plants. SO₂ emissions are known to not only cause health issues, but also have an adverse effect on the environment in various ways. Several Flue Gas Desulfurization (FGD) technologies have been incorporated in power plants. The most popular technology is Wet FGD, where a limestone slurry is used to absorb SO₂ from the flue gas. A detailed droplet scale model describing the instantaneous and finite rate chemistry is developed. The ill-posed Differential-Algebraic Equation (DAE) droplet model is reformulated to a well-posed index-1 DAE through index reduction. The droplet model is integrated with the bulk phase by incorporating gas-liquid mass transfer, and an oxidation reactor model to simulate the dynamic operation of the counter-current spray scrubber. As a result, the model has a well-conditioned Jacobian and overcomes the modeling challenges of previous works and enables numerical solution without requiring carefully selected initialization or specialized solution procedures. The model is successfully validated using power plant measurements, and nonlinear model predictive control (NMPC) studies are demonstrated to optimize recycle stream flowrates to minimize pumping costs.

© 2022 The Authors. Published by Elsevier Ltd. This is an open access article under the CC BY-NC-ND license (<http://creativecommons.org/licenses/by-nc-nd/4.0/>).

1. Introduction

Emission of sulfur dioxide present in the flue gas from coal-fired power plants not only causes health hazards, but also has an adverse impact on the environment leading to air, soil and water acidification. As a direct consequence, many countries have placed strict regulations on SO₂ emissions. Various flue gas desulfurization (FGD) technologies are available to reduce these emissions. The most popular technology is the wet limestone FGD (WFGD) because of its high SO₂ removal efficiency and low capital and operating costs. It employs a counter-current spray scrubber to absorb SO₂ in a limestone slurry, and involves a forced oxidation step to produce gypsum as a marketable byproduct (Nygaard

et al., 2004; Brogren and Karlsson, 1997). A schematic of limestone FGD scrubber is shown in Fig. 1. The WFGD system consists of two main sections: the absorption zone with spray headers, and the oxidation zone (slurry tank). Flue gas enters at the bottom of the spray tower above the slurry tank. It flows upwards and comes in counter-current contact with the droplets containing limestone slurry descending from spray nozzles. The slurry drops enter the absorption zone typically over several spray levels, each with a dedicated recirculation pump. They react with the flue gas and collect in the slurry tank. The overall reactions are represented as:



Despite the simple overall reactions, the component chemistry is complex. Several species, including ionic species, play an important role in the chemistry through instantaneous as well as

* Corresponding author.

E-mail address: biegler@cmu.edu (L.T. Biegler).

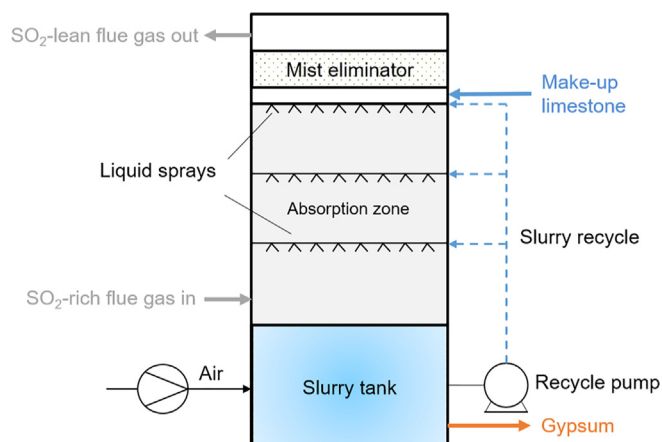


Fig. 1. Schematic of a wet FGD scrubber.

rate-limiting reactions. There are four main processes occurring in the system: limestone dissolution, SO_2 absorption, sulfite oxidation and gypsum (CaSO_4) crystallization (Brogren and Karlsson, 1997; Zhong et al., 2008). The oxidation and crystallization occur mainly in the slurry tank. Due to high recycle slurry to gas ratio, the limestone dissolution is assumed to be at equilibrium.

Several FGD models for the limestone based system have been developed at different levels of abstraction. Simple equilibrium models were developed to characterize the FGD process as a 1-D model (Lowell et al., 1970). Several studies have focused on modeling the species chemistry and hydrodynamics in the absorption zone (Brogren and Karlsson, 1997; Chang and Rochelle, 1981; Gage, 1989; Gage and Rochelle, 1992). These works primarily focus on a phenomenological description of the slurry droplets in the absorption zone of the FGD unit. The chemistry model for SO_2 absorption can lead to a high-index DAE system. When solving these DAE models numerically, they are characterized by an ill-conditioned Jacobian and are, therefore, not suitable for Newton-based methods. Custom solution procedures may be required with careful initialization to solve such models. For example, Brogren and Karlsson (1997) use the multivariate Gauss-Newton method iteratively to estimate individual species concentrations from specified concentration of aggregated species, before numerically integrating the DAE using DDASSL (Petzold, 1982). While such customized solution procedures and initialization can be used for simulation, there are considerable difficulties and computational expense in using those approaches for solving optimization problems, especially dynamic optimization.

Other works incorporate the slurry tank dynamics with the droplet and bulk phases in the absorption zone. Nygaard et al. (2004) provide experimental measurements of the gas and slurry phases in the FGD scrubber. Zhong et al. (2008) simplify the chemistry and apply a Lagrangean framework to extend the droplet model throughout the absorption zone. Neveux and Le Moulec (2011) integrate the detailed droplet chemistry with the bulk gas phase and incorporate the dynamics of the slurry tank into the model.

Efficient control of the FGD operation is not only important for satisfying critical emission constraints, but also for maximizing energy efficiency of the process. While spray towers are one of the simplest to construct and operate, they suffer from high pumping costs due to high recycle slurry to gas ratios compared to other types of contactors used in WFGD processes. As the SO_2 load to the spray tower changes during dynamic operation, it provides opportunities for minimizing the pumping costs by manipulating the spray flowrates at each spray header. While larger flowrates at the lowest spray level can reduce pumping cost, it also reduces

SO_2 removal efficiency. Therefore, it is desired to design the control system for minimizing the pumping cost without violating SO_2 removal constraint in the face of changing flue gas flowrates. Very few studies exist that address dynamic optimization and NMPC of the FGD operation. Guo et al. (2019) develop a simplified FGD model based on transfer units analogous to general separation unit operations, and use a metaheuristic approach to optimize process parameters under typical load conditions. Villanueva Perales et al. (2009) apply an MPC strategy on a pilot-scale FGD system and report an improvement in set-point tracking and disturbance rejection compared to conventional feedback control. Huang et al. (2017) apply a constrained MPC approach on an ammonia-based FGD system to achieve a desired level of desulfurization efficiency. Liu et al. (2021) develop a detailed dynamic FGD model in which the liquid-gas contact is assumed to occur in a single contact zone below the spray headers. They add further simplifications to the model and apply an economic NMPC strategy to optimize the operating costs while satisfying emission standards.

This work focuses on the development of a well-posed, dynamic DAE model for the absorption of SO_2 in the limestone slurry. The model takes into account the phenomenological description of the FGD system as done by previous works, incorporates the droplet and bulk phases with the slurry tank dynamics, and is tenable for dynamic optimization and NMPC studies. In the next section, we describe the complex chemistry of the FGD scrubber. In Section 3, we present the system of coupled differential and algebraic equations that describe the SO_2 absorption in a limestone slurry droplet based on penetration theory. We analyze the challenges associated with the numerical solution of the absorption model and provide a detailed reformulation procedure to obtain a model with a tractable numerical solution. In Section 4, we integrate the droplet model with the scrubber bulk and the slurry tank and simulate the dynamic FGD system. In Section 5, we present the results from simulations of the SO_2 absorption in a slurry droplet, as well as steady-state and dynamic simulations of the FGD scrubber. In Section 6, we demonstrate optimal control of the FGD system by applying an economic NMPC strategy to minimize the pumping costs while maintaining a desired level of scrubbing efficiency and rejecting dynamic load changes at different operating conditions.

2. Reaction system

While there can be many minor species in this system, there are 10 dominating species as given in Table 1. It should be noted that the modeling approach is general and readily extends to incorporate additional species.

The model takes into consideration both instantaneous equilibrium reactions of the slurry and reactions with finite rates.

2.1. Instantaneous reactions

The dissociation of dissolved SO_2 and HCO_3^- are instantaneous reactions (Brogren and Karlsson, 1997). The ion pairs of CaSO_3 and CaCO_3 are also assumed to be at equilibrium.

Table 1
Species considered.

1.	H^+	6.	CO_3^{2-}
2.	Ca^{2+}	7.	CO_2
3.	HSO_3^-	8.	SO_2
4.	HCO_3^-	9.	CaCO_3
5.	SO_3^{2-}	10.	CaSO_3



2.2. Finite rate reactions

The hydrolysis of CO_2 is a slow reaction: $\text{CO}_2 \xrightarrow{\text{H}_2\text{O}} \text{H}^+ + \text{HCO}_3^-$. The rate can be expressed as the difference between forward and backward reaction rates, with rate constants k_1 and k_2 respectively. Also, C_i is the concentration of species i .

$$r_{\text{CO}_2} = k_2 C_{\text{H}^+} C_{\text{HCO}_3^-} - k_1 C_{\text{CO}_2} \quad (3)$$

The equilibrium constant, K_{CO_2} is related to the reaction rates:

$$K_{\text{CO}_2} = \frac{k_1}{k_2} \frac{\gamma_{\text{H}^+} \gamma_{\text{HCO}_3^-}}{\gamma_{\text{CO}_2}} \quad (4)$$

Here γ_i is the activity coefficient of species i . Combining the above equations and defining activity $a_i = \gamma_i C_i$, we get the following relation (Wallin and Bjerle, 1989).

$$r_{\text{CO}_2} = k_1 C_{\text{CO}_2} \left(\frac{a_{\text{H}^+} a_{\text{HCO}_3^-}}{K_{\text{CO}_2} a_{\text{CO}_2}} - 1 \right) \quad (5)$$

The dissolution of limestone is also a slow reaction (Zhong et al., 2008): $\text{CaCO}_3 \xrightarrow{\text{H}_2\text{O}} \text{Ca}^{2+} + \text{CO}_3^{2-}$. The rate is given as follows.

$$r_{d,\text{CaCO}_3} = k_{d,\text{CaCO}_3} (\text{RS}_{\text{CaCO}_3} - 1), \text{ where } \text{RS}_{\text{CaCO}_3} = \frac{C_{\text{Ca}^{2+}} C_{\text{CO}_3^{2-}}}{K_{\text{SP},\text{CaCO}_3}} \quad (6)$$

Here, k_{d,CaCO_3} is the rate constant, $\text{RS}_{\text{CaCO}_3}$ is the relative supersaturation and $K_{\text{SP},\text{CaCO}_3}$ is the solubility product of calcium carbonate. In the next section, we introduce the spray scrubber model for the absorption of SO_2 .

3. SO_2 absorption model

Here, we describe the SO_2 absorption process based on penetration theory. It involves equilibrium expressions for the reactions (2) and mass balances for sulfite, carbonate, calcium, CO_2 and a charge balance. Here, $\nabla = d/dx$, where x is the radial distance from the center of the droplet. In Eqs. (7.6)–(7.10), S(IV) refers to sulfite species comprising HSO_3^- , SO_3^{2-} , CaSO_3 and SO_2 , C(IV) refers to carbonate species involving HCO_3^- , CO_3^{2-} , CaCO_3 and CO_2 , Ca refers to calcium species involving CaSO_3 , CaCO_3 and Ca^{2+} , and Chg refers to charged species constituted by positive and negative ions from Table 1. A separate material balance for CO_2 is included as its hydrolysis reaction is slow (Brogren and Karlsson, 1997).

$$\text{Equilibrium equations } K_{\text{SO}_2} C_{\text{SO}_2} = C_{\text{H}^+} C_{\text{HSO}_3^-} \quad (7.1)$$

$$K_{\text{HSO}_3^-} C_{\text{HSO}_3^-} = C_{\text{H}^+} C_{\text{SO}_3^{2-}} \quad (7.2)$$

$$K_{\text{HCO}_3^-} C_{\text{HCO}_3^-} = C_{\text{H}^+} C_{\text{CO}_3^{2-}} \quad (7.3)$$

$$K_{\text{CaSO}_3} C_{\text{CaSO}_3} = C_{\text{Ca}^{2+}} C_{\text{SO}_3^{2-}} \quad (7.4)$$

$$K_{\text{CaCO}_3} C_{\text{CaCO}_3} = C_{\text{Ca}^{2+}} C_{\text{CO}_3^{2-}} \quad (7.5)$$

Equations for the droplet phase

$$\frac{\partial C_{\text{S(IV)}}^{\text{tot}}}{\partial t} = \sum_{k=1}^4 \left(\mathcal{D}_k \cdot \nabla^2 C_k - \frac{2}{x} \mathcal{D}_k \cdot \nabla C_k \right), k = \text{Sulfite species} \quad (7.6)$$

$$\frac{\partial C_{\text{C(IV)}}^{\text{tot}}}{\partial t} = \sum_{k=1}^4 \left(\mathcal{D}_k \cdot \nabla^2 C_k - \frac{2}{x} \mathcal{D}_k \cdot \nabla C_k \right) + r_{d,\text{CaCO}_3}, k = \text{Carbonate species} \quad (7.7)$$

$$\frac{\partial C_{\text{Ca}}^{\text{tot}}}{\partial t} = \sum_{k=1}^3 \left(\mathcal{D}_k \cdot \nabla^2 C_k - \frac{2}{x} \mathcal{D}_k \cdot \nabla C_k \right) + r_{d,\text{CaCO}_3}, k = \text{Calcium species} \quad (7.8)$$

$$\frac{\partial C_{\text{CO}_2}}{\partial t} = \mathcal{D}_k \cdot \nabla^2 C_k - \frac{2}{x} \mathcal{D}_k \cdot \nabla C_k + r_{\text{CO}_2}, k = \text{CO}_2 \quad (7.9)$$

$$\frac{\partial C_{\text{Chg}}^{\text{tot}}}{\partial t} = \sum_{k=1}^6 q_k \left(\mathcal{D}_k \cdot \nabla^2 C_k - \frac{2}{x} \mathcal{D}_k \cdot \nabla C_k \right), k = \text{Charged species} \quad (7.10)$$

Here, q_k and \mathcal{D}_k are the charge and diffusivity of species k , respectively. At every level of height along the scrubber, the concentration profiles for the droplets are developed from the boundary conditions that evolve in the spray zones.

3.1. Boundary conditions

Due to symmetry, the flux of species at the center of the droplet is set to zero. The initial and boundary conditions are as follows:

$$\text{At } t = 0 \text{ and } x \in [0, R]: C_k = C_{k,0}, \sum q_k \mathcal{D}_k = 0$$

where k are the species and R is radius of the droplet. At $t > 0$ and $x = 0$ (center of the droplet):

$$J_{\text{S(IV)}} = J_{\text{C(IV)}} = J_{\text{CO}_2} = J_{\text{Ca}} = J_{\text{Chg}} = 0$$

At $t > 0$ and $x = R$ (in this model, we assume R to be fixed):

$$J_{\text{S(IV)}} = k_{G,\text{SO}_2} (P_{\text{SO}_2} - P_{\text{SO}_2}^{\text{int}}), J_{\text{CO}_2} = k_{G,\text{CO}_2} (P_{\text{CO}_2} - P_{\text{CO}_2}^{\text{int}}), J_{\text{C(IV)}} = J_{\text{Ca}} = J_{\text{Chg}} = 0$$

where P_{SO_2} and P_{CO_2} refer to the bulk phase pressures. Also, $P_{\text{SO}_2}^{\text{int}}$ and $P_{\text{CO}_2}^{\text{int}}$ are interfacial pressures, assumed in equilibrium with their slurry concentrations at the droplet boundary. In other words, at the surface of the droplet, we have a flux condition for the absorption of gases SO_2 and CO_2 . Since there is no absorption taking place for the other species, their flux at the surface is zero.

3.2. Modeling challenges

In this section, we consider the droplet model, i.e., the model that describes SO_2 absorption in a single slurry droplet. This is a steady-state model obtained by neglecting the time-dependent terms in equation (7). This is a differential-algebraic equation (DAE) model where the mass balance equations are the differential part and the equilibrium equations are the algebraic part. Upon examination of this system, we note that this DAE system is high-index, i.e., the singular structure of algebraic variables in the algebraic (equilibrium) system does not allow us to specify boundary conditions for the differential terms independently. First we reformulate the second order DAE to a first order system. Then we reformulate the DAE to an index-1 system.

3.2.1. First order reformulation

The first order reformulation of the differential equations of the steady-state model obtained from equation (7) is given below.

Equations for the droplet phase

$$\sum_{k=1}^3 \left(\mathcal{D}_k \nabla U_k - \frac{2}{x} \mathcal{D}_k U_k \right) + r_{d,\text{CaCO}_3} = 0, k = \text{Calcium species} \quad (8.1)$$

$$\mathcal{D}_k \nabla U_k - \frac{2}{x} \mathcal{D}_k U_k + r_{\text{CO}_2} = 0, k = \text{CO}_2 \quad (8.2)$$

$$\sum_{k=1}^4 \left(\mathcal{D}_k \nabla U_k - \frac{2}{x} \mathcal{D}_k U_k \right) = 0, k = \text{Sulfite species} \quad (8.3)$$

$$S_i = \sum_{s=1}^3 \bar{S}_{s,i} = \frac{1}{F_{\text{make-up}}} \sum_{s=1}^3 R_{s,i} \quad (14)$$

For a recycle ratio S_i at time t_i , the new concentrations of species k in stage s at level $l = 0$ (at the spray header) are calculated as follows.

$$C_{k,s,l=0,i} = \frac{1 + (s-1)\bar{S}_{s,i}}{1 + s\bar{S}_{s,i}} C_{k,s-1,l=n,i} + \frac{\bar{S}_{s,i}}{1 + s\bar{S}_{s,i}} C_{k,i}^{\text{recycle}} \quad (15)$$

The flux of SO_2 entering the droplet is given by

$$J_{\text{SO}_2} = k_{G,\text{SO}_2} (P_{\text{SO}_2} - P_{\text{SO}_2}^{\text{int}}) \quad (16)$$

Assuming that the interfacial pressure, $P_{\text{SO}_2}^{\text{int}}$, is in equilibrium with the slurry concentration of SO_2 at the boundary of the droplet, the flux of SO_2 into a droplet in stage s at level l at time t_i can be written as

$$J_{\text{SO}_2,s,l,i} = k_{G,\text{SO}_2} (P_{\text{SO}_2,s,l,i} - H_{\text{SO}_2} C_{\text{SO}_2,x=R,s,l,i}) \quad (17)$$

where H_{SO_2} is Henry's constant for SO_2 . From this flux, we can calculate the flow rate of SO_2 entering per unit volume of the droplet, as a function of the slurry concentration.

$$J_{\text{SO}_2,s,l,i}^V = \frac{3}{R} J_{\text{SO}_2,s,l,i} \quad (18)$$

Here, $3/R$ represents the surface area per unit volume of the droplet. Note that $J_{\text{SO}_2}^V$ corresponds to the total concentration of SO_2 absorbed in a level per unit time. The amount of SO_2 absorbed into a droplet in a stage is obtained from the flux of SO_2 into the droplet and its residence time t_s^r in stage s . The species balance for the SO_2 in the gas phase can be written as

$$F y_{\text{SO}_2,s,l,i} = F y_{\text{SO}_2,s,l+1,i} - \dot{n}_{\text{SO}_2,s,l,i}^{\text{abs}} \quad (19)$$

Here, y_{SO_2} is the mole fraction of SO_2 in the gas phase, and F is the flue gas flowrate. It can be noted that due to the very low concentration of SO_2 in the flue gas (in ppmv level), relative change in the flue gas flowrate through the spray tower is negligible. For a gas phase voidage ε , absorption rate in stage s for the control volume V_l can be written as

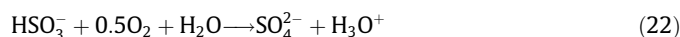
$$\dot{n}_{\text{SO}_2,s,l,i}^{\text{abs}} = J_{\text{SO}_2,s,l,i} 4\pi R^2 \frac{V_l}{\frac{4}{3}\pi R^3} (1 - \varepsilon) = J_{\text{SO}_2,s,l,i}^V V_l (1 - \varepsilon) \quad (20)$$

The mole fraction of SO_2 can be related to the total pressure as

$$P_{\text{SO}_2,s,l,i} = P y_{\text{SO}_2,s,l,i} \quad (21)$$

4.2. Slurry tank (oxidation reactor) model

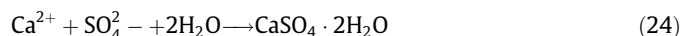
Sulfite oxidation and gypsum crystallization are the rate-limiting steps that occur in the slurry tank. Calcium sulfite in the slurry is converted to calcium sulfate by forced oxidation as follows.



The kinetic expression for the rate of oxidation is as follows (Karatzas et al., 2005).

$$r_{o,\text{HSO}_3^-} = k_o \left(a_{\text{HSO}_3^-} \right)^{3/2} \quad (23)$$

The gypsum precipitation reaction is written as



The kinetics are based on a semiempirical rate law as given below (Kiil et al., 1998).

$$r_{p,\text{CaSO}_4} = k_{p,\text{CaSO}_4} \left(\frac{a_{\text{Ca}^{2+}} a_{\text{SO}_4^{2-}}}{K_{S,\text{CaSO}_4}} - 1 \right) \quad (25)$$

The slurry tank is modeled as a CSTR of volume V . With the conversion from the oxidation and precipitation reactions given by X_o and X_p respectively, the mass balance is written as

$$V \frac{dC_{\text{HSO}_3^-}}{dt} = F_{\text{HSO}_3^-}^{\text{in}} X_o - r_{o,\text{HSO}_3^-} V \quad (26.1)$$

$$V \frac{dC_{\text{Ca}^{2+}}}{dt} = F_{\text{Ca}^{2+}}^{\text{in}} X_p - r_{p,\text{CaSO}_4} V \quad (26.2)$$

Here, F^{in} is the molar flow rate of the slurry into the reactor. The rate constants are taken from (Neveux and Le Moulec, 2011). The concentration of HSO_3^- and Ca^{2+} can be written in terms of conversion as

$$C_{\text{HSO}_3^-} = C_{\text{HSO}_3^-}^{\text{in}} (1 - X_o), \quad \text{and} \quad C_{\text{Ca}^{2+}} = C_{\text{Ca}^{2+}}^{\text{in}} (1 - X_p) \quad (27)$$

Here C_k^{in} is the concentration of species k entering the oxidation reactor. The mass balance equations can thus be solved for the conversions X as follows.

$$- \left(C_{\text{HSO}_3^-}^{\text{in}} \right) \frac{dX_o}{dt} = \frac{F_{\text{HSO}_3^-}^{\text{in}}}{V} X_o - r_{o,\text{HSO}_3^-} \quad (28.1)$$

$$- \left(C_{\text{Ca}^{2+}}^{\text{in}} \right) \frac{dX_p}{dt} = \frac{F_{\text{Ca}^{2+}}^{\text{in}}}{V} X_p - r_{p,\text{CaSO}_4} \quad (28.2)$$

A portion of the solution from the slurry tank goes into the recycle stream which is fed to the three spray headers. After determining the concentrations of HSO_3^- , Ca^{2+} and H^+ from the slurry tank model, the recycle slurry concentrations of the other species are calculated assuming equilibrium given by Eqs. (7.1)–(7.5).

5. Simulation results and discussion

In this section, we present the results from simulations of the droplet model for SO_2 absorption and the steady-state and dynamic simulation of the scrubber.

5.1. SO_2 absorption in a slurry droplet

As discussed before, the degrees of freedom for the droplet model involve the variables U_k, \forall species k , concentrations C_k for $k = \text{SO}_2, \text{CO}_2, \text{CaSO}_3, \text{H}^+, \text{CO}_3^{2-}$, as well as the partial pressures of SO_2 and CO_2 . The partial pressures are treated as parameters in the droplet model, but are unknowns and calculated as part of the scrubber model. The parameters used are shown in Table 2. The values for the radius and partial pressures are inferred from Brogren and Karlsson's work (Brogren and Karlsson, 1997), while the boundary conditions are estimated from their results. We discretized the radial coordinate of the droplet in Pyomo (Hart et al., 2011; Hart et al., 2017) using orthogonal collocation on finite elements. The number of finite elements is 10, with 3 collocation points in each element. Lagrange-Radau collocation results in 31 points on the radial coordinate and leads to a problem size of about 1500 equations and variables. We simulated the mass transfer process into the droplet by solving the DAE system described in Section 3 using IPOPT (Wächter and Biegler, 2006). The results from the simulations are illustrated in Figs. 6–9. The profiles show the concentration changes of a species from center to surface of the slurry droplet. The profile for SO_2 shows about a 30% drop in concentration across the radius of the droplet.

Fig. 10 compares the concentration profile for total sulfite for our model as well as those reported by Brogren and Karlsson (1997) for similar droplet size and operating conditions. In their work, they report time-dependent profiles for penetration times

Table 2
Boundary conditions and parameters.

Variable	Value
$C_{k,x=0}$ for $k = \text{CO}_2, \text{CaSO}_3, \text{H}^+$	$5 \times 10^{-4} \text{ M}$
$C_{k,x=0}$ for $k = \text{SO}_2, \text{CO}_3^{2-}$	$1 \times 10^{-5} \text{ M}, 5 \times 10^{-9} \text{ M}$
$U_{k,x=0} \forall k \sim \{\text{SO}_2, \text{CO}_2\}$	0
$D_g U_{g,x=R}$ for $g = \text{SO}_2$ and CO_2	$-k_{G,g}(P_g - P_g^i)$
P_{SO_2}	200 Pa
P_{CO_2}	10 Pa
R	$5 \times 10^{-4} \text{ m}$

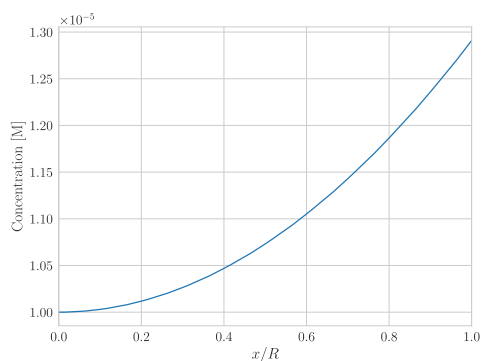
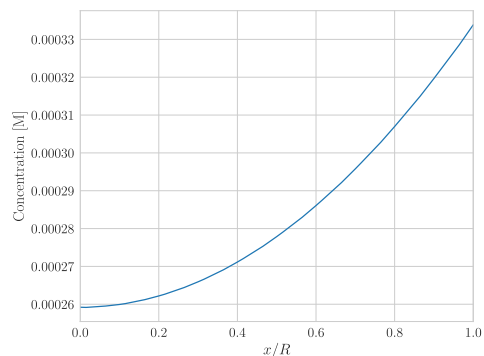
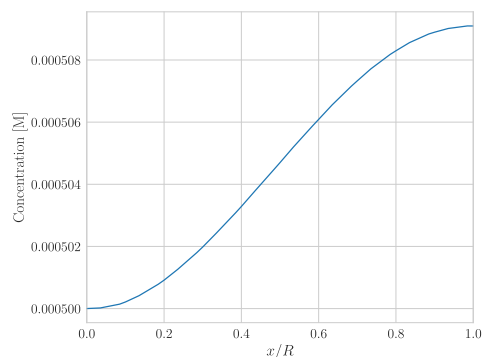
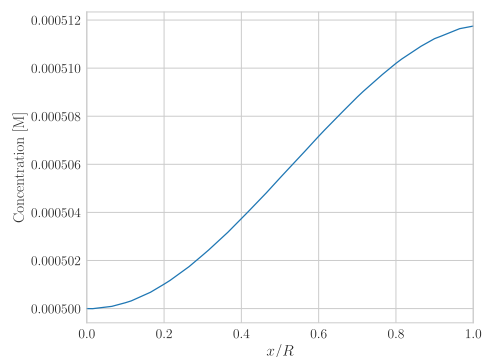
of up to 0.2s, while our model results show only steady-state profiles. Note that both sets of concentration profiles have a similar characteristic with increasing penetration depths of sulfite starting from the droplet surface. We note that the operating conditions used in their work vary slightly from those used here. Nevertheless, Fig. 10 shows the normalized concentration profiles of total sulfite at three simulation times, along with the steady-state profile from this study. The normalized concentrations of the aggregated species k are calculated from the boundary concentrations as follows.

$$\bar{C}_{k,x} = \frac{C_{k,x} - C_{k,x=0}}{C_{k,x=R} - C_{k,x=0}}$$

From the figure, we note that the penetration depth $(1 - x/R)$ is very small initially and expands with the evolution of time. Our steady-state profile is quite consistent with this evolution.

5.2. Steady-state scrubber simulation

The steady-state model simulates the SO_2 scrubbing in the absorption zone. The droplet model given by Eqs. (7.1)–(7.5), (8.1)–(8.5), (9.1)–(9.5) and (10), and the bulk phase (11)–(21) constitute the steady-state model. To determine n , we perform mesh refinement studies for various values of n from 3 to 15, with the solution at $n = 15$ chosen as reference for model accuracy. For n values below 5, the resulting SO_2 removal efficiency deviated from the reference solution by up to 5%, while there was negligible difference in accuracy for $n = 5$ (0.0001%). This is illustrated in Fig. 11. Computation time for $n = 3$ was 5.8s, and increases to 400s for $n = 15$. Hence, we chose $n = 5$, as a larger n incurs high computational cost but does not change the solution significantly. Also, the resulting residence time of droplets in a level is sufficient for the slow reactions to reach equilibrium. Unless otherwise specified, we use the values of operating parameters shown in Table 3 for the simulations. All simulations are implemented in Pyomo (Hart et al., 2011; Hart et al., 2017). The radial coordinate in the droplets is discretized using orthogonal collocation on finite elements. As

**Fig. 6.** Concentration profile of SO_2 .**Fig. 7.** Concentration profile of HSO_3^- .**Fig. 8.** Concentration profile of CaSO_3 .**Fig. 9.** Concentration profile of H^+ .

mentioned before, the absorption zone is made up of three stages defined by three spray headers. Each stage is further discretized into $n = 5$ sub-stages. The discretized model is solved using IPOPT (Wächter and Biegler, 2006).

The purpose of the steady-state simulations is to evaluate the sensitivity to partial pressure of SO_2 that is expected to vary as the sulfur composition in coal and/or the air to fuel ratio in the boiler changes with load. First, we simulate the scrubber for a fixed recycle ratio of $S = 1$. The make-up slurry concentration of SO_2 is $1 \times 10^{-5} \text{ mol/L}$. The SO_2 removal efficiency for different recycle stream concentrations of SO_2 is illustrated in Fig. 12. In all cases, the efficiency increases for high inlet SO_2 partial pressures, as the SO_2 pressure in the bulk through the entire spray tower remains at a relatively higher value. This improves the driving force for gas-liquid mass transfer. The profiles indicate that the efficiency is higher for lower recycle concentration of SO_2 over the range of pressures. This is to be expected because a lower slurry concentra-

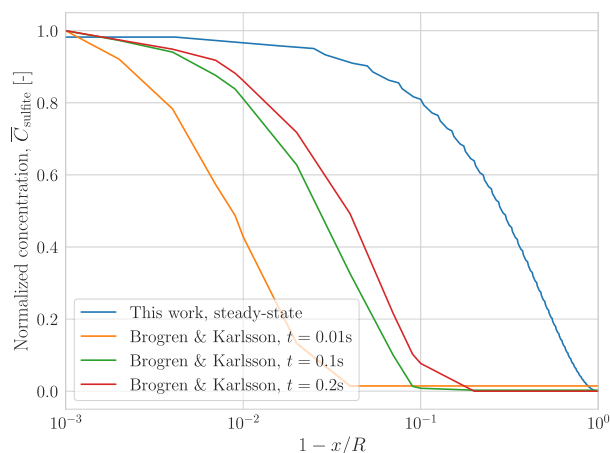


Fig. 10. Comparison of the droplet concentration profiles of total sulfite reported by Brogren and Karlsson (1997) and the steady-state profile in this work.

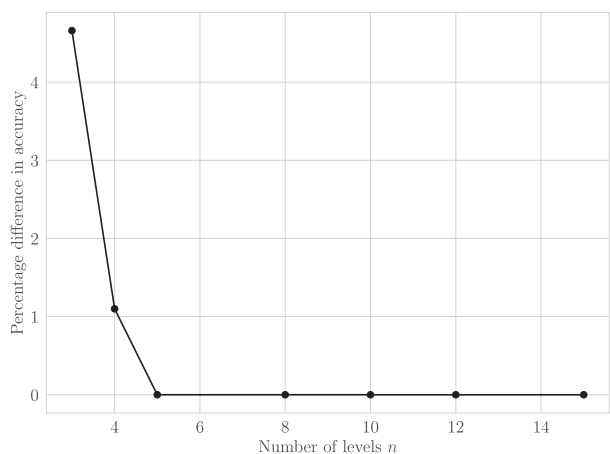


Fig. 11. Selection of n : difference in accuracy for efficiency calculation compared to $n = 15$.

Table 3
Parameters for scrubber simulation.

Variable	Value
D_s (diameter of scrubber)	6.0 m
h_s	1.5 m
ε	0.7
S	1.5
F	8.47 kmol/s
F^{in} (slurry flowrate entering slurry tank)	3041.64 L/s
V	1200 m ³
P_{SO_2} at scrubber inlet	80 Pa
P_T (total pressure of flue gas)	78 kPa
y_{SO_2} at scrubber inlet	0.001236

tion would result in a higher driving force for gas-liquid mass transfer as well as a higher reaction rate, and consequently a higher scrubbing rate in each sub-stage. The figure also includes the case with zero recycle ($S = 0$), i.e., when the slurry solution from the tank is not pumped back to the spray headers, and only fresh slurry is fed at the top of the scrubber. In this case, the model gives high efficiency of SO_2 removal over the range of SO_2 partial pressures in the incoming flue gas, as seen from the figure. Further, the efficiency is consistently lower than the case when the recycle concentration is the same as the make-up slurry SO_2 concentration due to a lower total flowrate. Compared with the case when the

recycle SO_2 concentration is 1×10^{-5} mol/L, the efficiency for $S = 0$ is higher at low pressures as the concentration of the reactants is higher and that of the products is lower leading to higher mass transfer and reaction rates. On the other hand, at high pressures, the efficiency for $S = 0$ is lower. This is because a higher total flowrate and SO_2 pressure results in larger driving forces, especially in the lower stages of the scrubber, which further improves scrubbing efficiency.

Fig. 13 shows the scrubbing efficiency for different recycle ratios for a given recycle stream concentration of SO_2 fixed at 1×10^{-4} mol/L. The recycle ratio S was changed by keeping the make-up slurry flowrate fixed at 500 L/s and adjusting the recycle stream flowrate. For low SO_2 partial pressure in the incoming flue gas, a smaller recycle ratio gives a better efficiency. This is again because the concentration of reactants is higher and the concentration of products is lower, leading to a higher mass transfer rate and reaction rate. For higher SO_2 pressures, the efficiency is relatively higher for larger recycle ratios. The reason for this relates to the relative fluxes at the gas-liquid interface near the top and bottom regions of the scrubber. The lower stages typically scrub SO_2 to a greater extent (this will be illustrated further in the next section), and a higher SO_2 partial pressure further improves scrubbing efficiency due to larger driving forces.

5.3. Dynamic scrubber simulation

The dynamic scrubber model involves integrating submodels of the droplet phase, bulk phase and the oxidation reactor and solving the resulting system of equations simultaneously. It is important to note that the droplet and bulk phase models (i.e., the submodels in the absorption column) operate at faster time-scales compared to the oxidation reactor. So, algebraic equations (with respect to time) are used for these submodels, and the oxidation reactor equation (28) is the only dynamic component in the FGD model. For a recycle ratio $S = 0.5$, we simulate the dynamic model and obtain the mole fraction profiles of SO_2 in the flue gas (y_{SO_2}). This is illustrated in Fig. 14. A time horizon of 7000s is chosen as it allows the model to reach steady-state for different operating conditions. This is important in the context of NMPC. The slow dynamics of the oxidation reactor allow for coarser mesh sizes, so the time coordinate is discretized into 5 finite elements. Fig. 14 shows the axial profiles of y_{SO_2} for each time point. For each profile, most of the SO_2 gets scrubbed in the bottom stage. This is due to a higher mass transfer flux in this region. The SO_2 concentration in the make-up slurry is 1×10^{-5} mol/L and this gives the blue line in Fig. 14. As the slurry becomes more saturated with SO_2 , the effective inlet slurry concentration increases due to recycle. This results in a lower average mass transfer flux and a lower removal efficiency represented by the orange line. As the slurry concentration gets constantly updated, the y_{SO_2} profile converges, representing 97% removal of SO_2 . Fig. 15 shows the SO_2 concentration profiles in slurry droplets at the flue gas inlet and outlet of the FGD scrubber. At any arbitrary time point, these plots illustrate the level of absorption and slurry saturation throughout the height of the scrubber. The slurry saturation is low at the top of the unit, and as it comes in contact with SO_2 in the flue gas, it gets more and more saturated. Overall, the FGD model is consistent with current operations and has been validated with plant data in an internal proprietary study.

6. Nonlinear model predictive control

In this section, we demonstrate optimal control of the FGD system by applying nonlinear model predictive control (NMPC) on some practical case studies. Nonlinear control methods typically require systematic design procedures that are intractable when

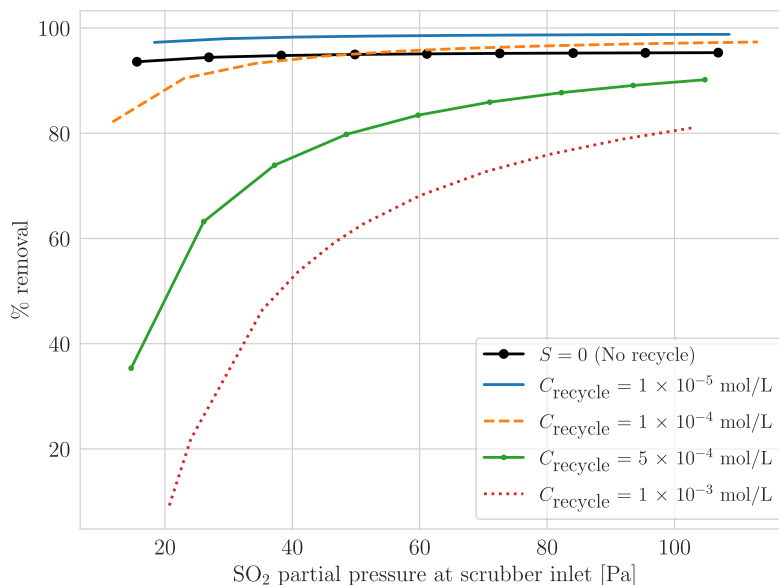


Fig. 12. Percentage removal of SO₂ for fixed recycle ratio ($S = 1.0$).

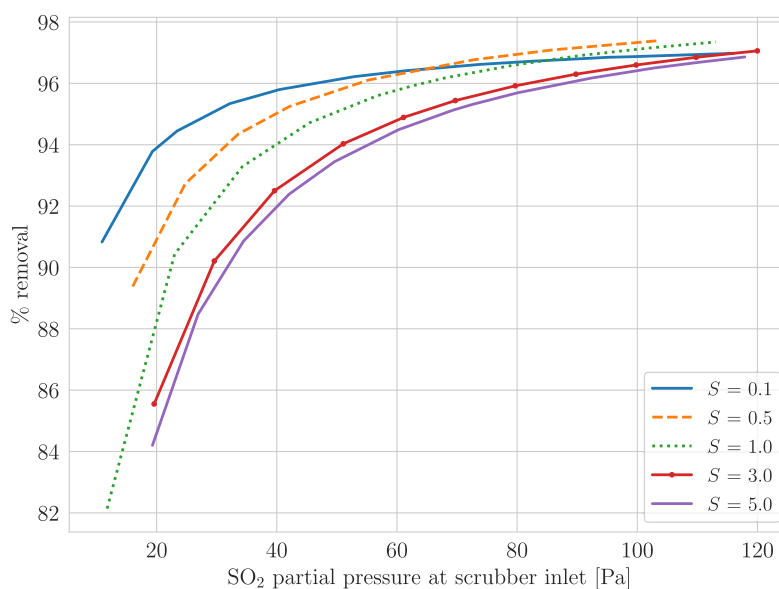


Fig. 13. Percentage removal of SO₂ for $C_{\text{recycle}}^{\text{SO}_2} = 1 \times 10^{-4}$ mol/L.

handling large-scale systems. NMPC is an online application of dynamic optimization where the control problem is stated as a constrained optimization. The NMPC generally involves a simultaneous simulation and dynamic optimization strategy. The control problem is formulated as an online finite horizon optimal control problem subject to the dynamic physical constraints (model equations), as well as constraints involving state and control variables (Findeisen and Allgöwer, 2002). In general, the model takes input measurements at time t_i and predicts an optimal control variable trajectory over a prediction horizon. An estimator uses the predicted control action to infer the values of state variables. These are then used by the control problem to predict the optimal control trajectory for the next time step (Patwardhan et al., 1990). Such a moving horizon estimation strategy is typically solved until we reach the prediction horizon.

In the dynamic simulation, as seen from Fig. 14, we note that a large fraction of SO₂ scrubbing takes place in the lowest spray zone, and especially so for low slurry saturation levels. This indicates an

opportunity to optimize pumping costs where we can expect to pump most of the recycle slurry to the lowest spray header, and the least slurry to the highest. For our case study, the goal is to determine the optimal recycle stream flowrates going to each spray header in response to disturbances in the flue gas flowrate, while achieving a high SO₂ removal efficiency. The recycle stream flowrates are indicated in Fig. 16. One way of incorporating this condition is to specify that at least 95% of SO₂ should be scrubbed at all time steps. Several other formulations of such a condition are possible. For example, we may enforce the average removal efficiency over fixed consecutive time periods to be above a certain threshold. For our model, we choose the former formulation as it represents a tighter restriction to satisfy environmental regulations. The constraint is written as:

$$y_{\text{SO}_2, \text{out}, i} - (1 - 0.95)y_{\text{SO}_2, \text{in}, i} \leq 0 \quad (29)$$

Solving the NMPC problem with the state inequality constraint such as (29) is vulnerable to nonrobustness of the NMPC. In other words,

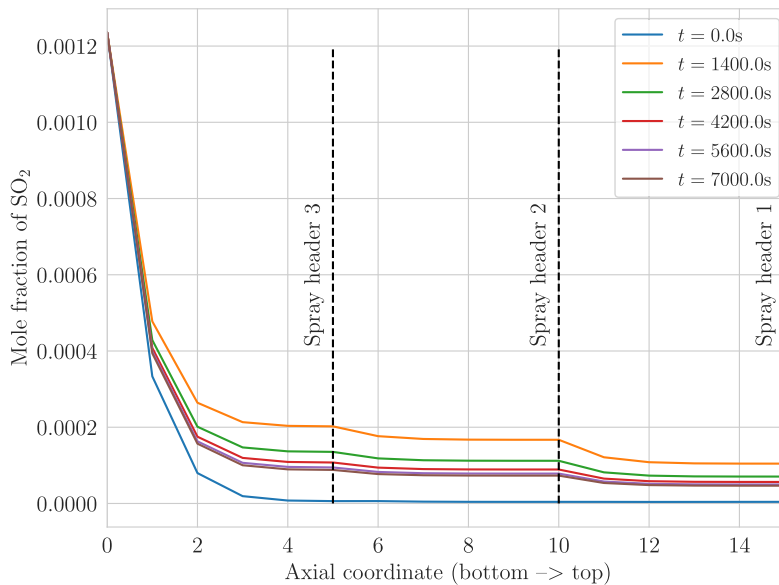


Fig. 14. Percentage removal of SO₂ for fixed recycle concentration.

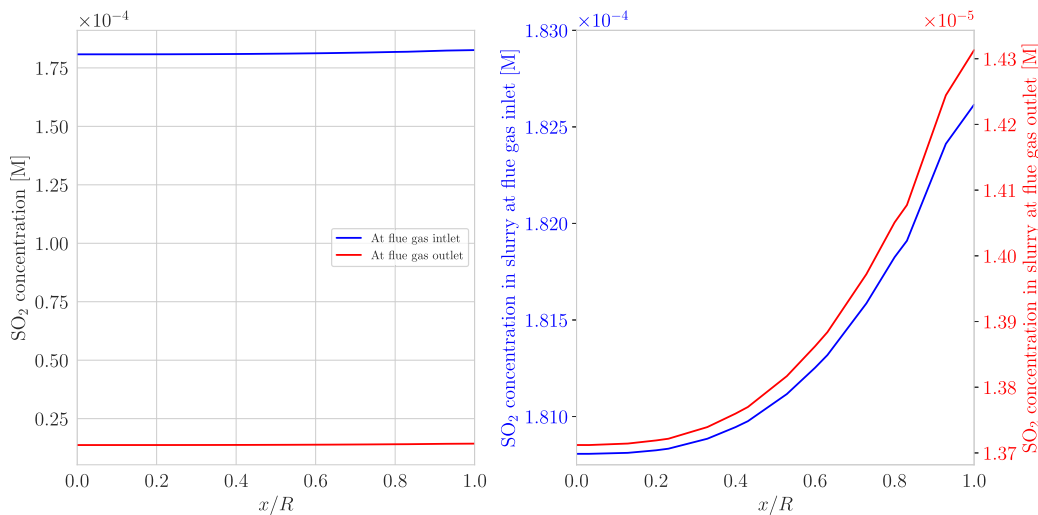


Fig. 15. Droplet SO₂ profiles at $t = 1400s$ at the flue gas inlet and outlet. On the left, these profiles are shown on a common scale and emphasize the difference in their magnitudes. On the right, the profiles are plotted on their respective scales to illustrate the absorption of SO₂ across the radial coordinate.

through perturbations in the inputs, such formulations lead to infeasibility of Eq. (29), thus leading to failure of the NMPC algorithm (Yang et al., 2015). To avoid this, an ℓ_1 -penalty relaxation of this constraint in equation (30) maintains robustness of the controller by treating it as a soft constraint with artificial variables p_i .

$$y_{SO_2,out,i} - (1 - 0.95)y_{SO_2,in,i} \leq p_i \tag{30.1}$$

$$p_i \geq 0 \tag{30.2}$$

To formulate the economic objective, we include the pumping costs for the three spray headers ($s = 1 \dots 3$). The NMPC problem formulation is:

$$\min \rho \sum_i p_i + \sum_i \sum_s \alpha_s R_{s,i} \tag{31.1}$$

$$\text{s.t. } z_{i+1} = f(z_i, R_{s,i}; F_i), \quad i = 1, \dots, N - 1, s = 1 \dots 3 \tag{31.2}$$

$$z_0 = X(t_k) \tag{31.3}$$

$$y_{SO_2,out,i} - (1 - 0.95)y_{SO_2,in,i} \leq p_i, \quad p_i \geq 0 \tag{31.4}$$

$$R_{s,i} \in \mathbb{U} \tag{31.5}$$

The first term in the objective is the ℓ_1 -penalty term with $\rho = 10^4$ selected as the penalty weight. The second term represents the stage cost, with weights α_s related to the pumping costs for the recycle flowrate $R_{s,i}$ at time t_i . The value for α_s is chosen as the height (in metres) of the spray header s from the ground. These heights are $\alpha_1 = 22.5, \alpha_2 = 21$ and $\alpha_3 = 19.5$ (Neveux and Le Moullec, 2011). The function f denotes the dynamic FGD model with states z_i , controls $R_{s,i} \forall s$, and input parameter F_i (flue gas flowrate) at time step t_i in the horizon. N is the number of time steps in the horizon. At time t_k in the plant, the initial conditions for the NMPC problem (31) are given by $X(t_k)$, and equation (30) gives the SO₂ specification. \mathbb{U} is a set representing the bounds on the control variables. The total horizon over which the studies are conducted is 12,600s, while the finite horizon for the moving horizon NMPC is 7000s. This horizon is discretized into 5 sampling times. We add a low frequency fluctuation to the nominal flue gas flowrate of 8.47 kmol/s for the initial 7000s horizon, after which it remains constant. The input flowrates are shown in Table 4 and Fig. 17. While the flue gas flowrate changes with time in Fig. 17, we assume that the NMPC

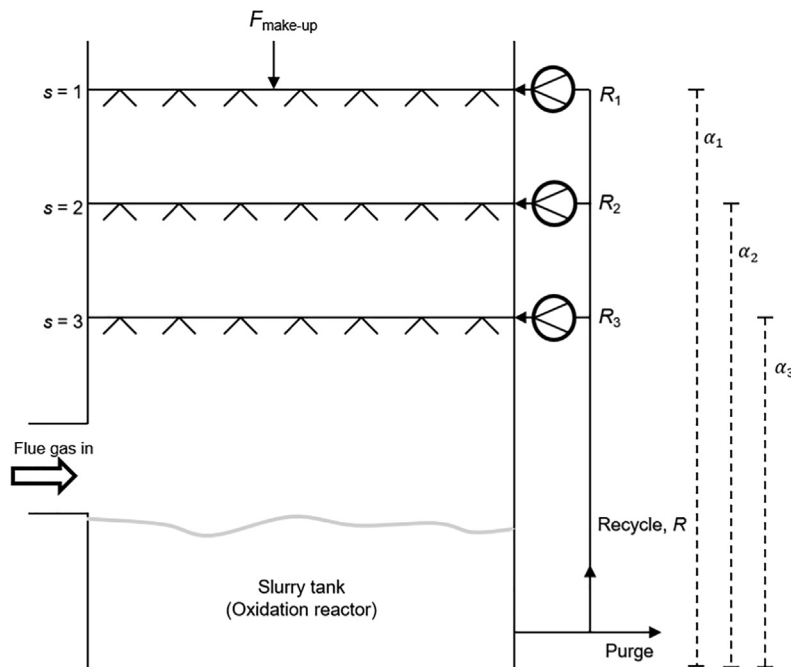


Fig. 16. Recycle stream flowrates are controls for the NMPC problem.

controller is unaware of changes to this flowrate. Consequently, the controller can only work with the current value of this flowrate, unless accurate feedforward information can be provided. Otherwise, this lack of information can lead to a suboptimal control trajectory over the horizon. Nevertheless, as time evolves, these control trajectories will be corrected through feedback as the actual flue gas flow rates are realized. Moreover, the results in this study do not include measurement noise nor model mismatch, which needs to be deferred to future work.

We solve the dynamic simulation problem at the nominal flue gas flowrate to obtain the initial steady-state for the state variables X . The initial conditions are $X_o = 0.68$ and $X_p = 0.22$ for the oxidation and precipitation reactions from equation (28), respectively. The flowrate of solution extracted from the oxidation tank that is sent to solids handling is taken to be 500 L/s. Since no accumulation is assumed, the make-up slurry flowrate is also set at 500 L/s. The flowrate of slurry entering the oxidation reactor is specified as 48280 GPM (or 3041.64 L/s). This results in a total recycle flowrate of 2541.64 L/s, which is divided into the three streams with flowrates R_1, R_2 and R_3 and gives an upper bound to these controls.

The dynamic FGD model is comprised of droplet constraints from Eqs. (7.1)–(7.5), (8.1)–(8.5), (9.1)–(9.5) and (10) at all points in space and time, bulk model from Eqs. (11)–(21), and the oxidation reactor model from Eqs. (23), (25) and (28). Starting at $t_0 = 0$, we solve the control problem (31) with the nominal steady state as the initial condition and the first input $F = 12.05$ kmol/s. For this input, the control problem is solved for a finite horizon of 7000s

Table 4
Flue gas flowrate (input).

Time	F (kmol/s)
0.0	12.05
1400.0	9.35
2800.0	8.67
4200.0	4.75
5600.0	7.92
≥ 7000.0	7.76

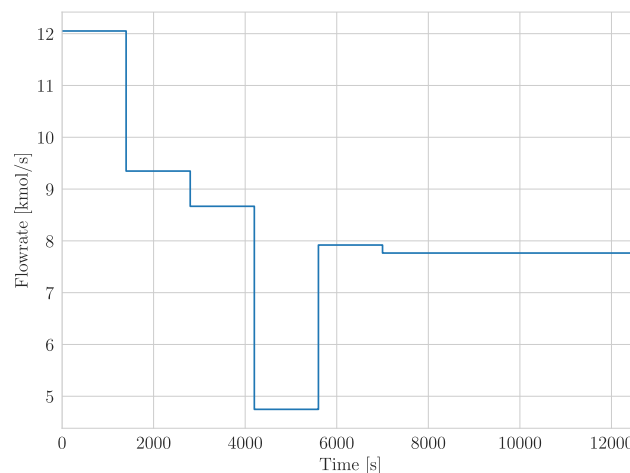


Fig. 17. Flue gas flow rate (external input to FGD).

to obtain the optimal control trajectory of the control variables (R_i). The first control action from the trajectory is transferred to the process model, after which we update the initial condition and move to the next time step. The control problem takes in the new input $F = 9.35$ kmol/s and the finite horizon moves forward by one time step. This process is repeated for each step and the control action is updated in each iteration. The optimal control profiles (recycle flowrates) and SO_2 removal are illustrated in Fig. 18.

Each iteration of NMPC is solved within the sampling time. After the flue gas flowrate remains constant at 7000s, the solution reaches steady-state in one time step. The results indicate that the optimal recycle flowrates are consistently higher for the lowest spray header, and they decrease in magnitude as we move upwards. This is expected behavior since we penalize the flowrates in proportion to the height of their corresponding spray header. As the flue gas flowrate decreases, the model increases the recycle flowrate at the lowest spray header (R_3) and decreases the recycle flowrate to the highest header (R_1). For the case when $F = 4.75$

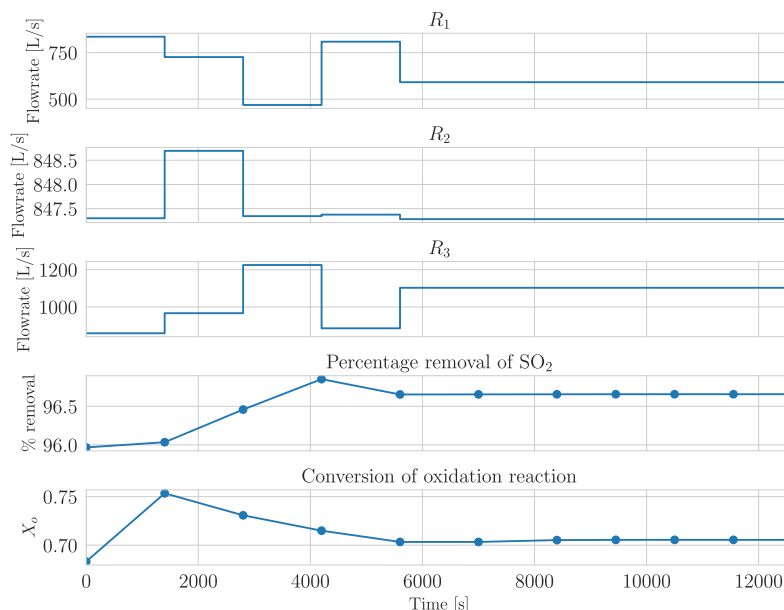


Fig. 18. Recycle flowrates, SO_2 removal profile and conversion of oxidation reaction for make-up slurry flowrate = 500 L/s.

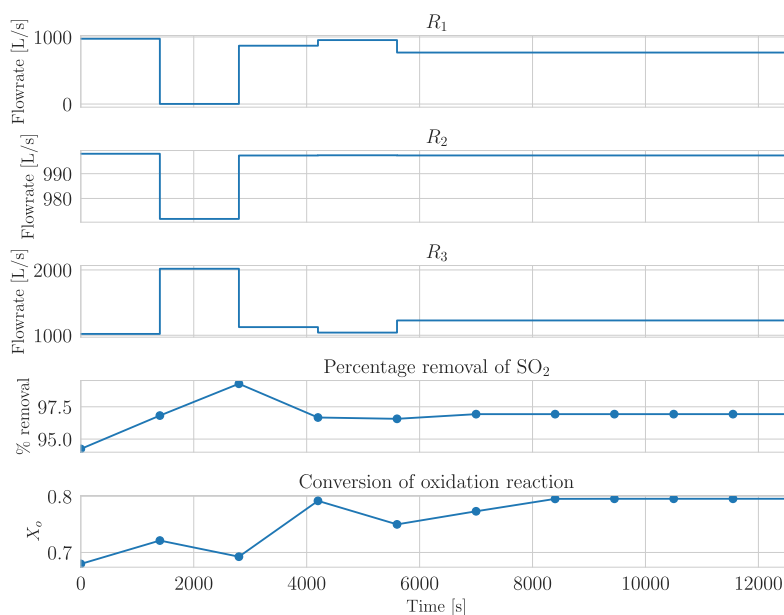


Fig. 19. Recycle flowrates, SO_2 removal profile and conversion of oxidation reaction for make-up slurry flowrate = 50 L/s.

kmol/s, the model seems to increase R_1 compared to the previous step. When the make-up slurry flowrate is 50 L/s, the optimal control profiles are shown in Fig. 19. We see similar behavior in terms of the relative share of each recycle flowrate. It is important to note that the weights in the objective function play a role in the optimization problem and the choice of these weights may differ depending on the economic goal. Also, the artificial variables p_i are always driven to zero and the environmental constraint equation (30) is satisfied at each point in time.

To evaluate these results, we consider two operating specifications: one where the entire recycle slurry is sent to the top spray header ($R_1 = R_2 = R_3 = 0$), and one where the recycle slurry is equally distributed to the three spray headers ($R_1 = R_2 = R_3 = R/3$). The resulting relative pumping costs for these cases are compared with the NMPC solutions in Table 5, with

the case with equally distributed flowrates chosen as reference. In order to enforce the SO_2 specification constraint equation (30) on the two operating scenarios, the upper bound on the total recycle flowrate R_i for these two scenarios is removed. The results also include relative pumping costs for these scenarios where the total recycle is fixed to the same value as for the NMPC cases and equation (30) is not enforced.

When the SO_2 specification is enforced at each time point, the results show that the average pumping costs resulting from the NMPC approach is lower compared to the two other operating scenarios. The NMPC cases represent a reduction of about 1.5% in the stage cost compared to the reference scenario, and will result in significant reduction in operating costs over long periods of operation. Further, both operating scenarios require a higher total recycle flowrate compared to the NMPC solution. Specifically, for the

Table 5
Relative costs of the operating scenarios.

Equation (30)	Make-up slurry flowrate	Relative costs		
		Only R_1	$R_1 = R_2 = R_3$	NMPC
Enforced	500 L/s	1.145	1.000	0.985
	50 L/s	1.149	1.000	0.986
Not enforced	500 L/s	0.923	0.860	
	50 L/s	0.922	0.860	

case where all the recycle is sent to the top spray header, the average recycle flowrate required is 18% higher than the NMPC approach. For the case with equally distributed flowrates to the three spray headers, the average recycle flowrate is 10% higher than the NMPC approach. For the last two cases, the average pumping costs are lower for the two scenarios compared to the first two cases. This is expected as equation (30) is not enforced for these cases. This demonstrates that the NMPC approach is able to derive control actions that result in lower costs and better performance compared to arbitrary operating specifications.

7. Conclusion

In this work, we have presented a detailed multiscale dynamic model for flue gas desulfurization. The complex chemistry and assumptions used to model the FGD scrubber have been discussed. At the droplet scale, the detailed chemistry model is reformulated to a well-posed index-1 DAE. At the bulk scale, the droplet model is incorporated by taking into account gas phase interactions. The reformulated DAE scrubber model enables tractable numerical solution using Newton-based methods such as IPOPT and does not require specialized solution strategies. The dynamic model was simulated and validated successfully using power plant measurements. From the dynamic simulations, it appears that most of the SO_2 in the flue gas is absorbed in the lowest spray stage, and the extent of absorption decreases as we move to higher stages. This opened up opportunities for optimal control through NMPC with the goal of minimizing the operating costs while achieving the required extent of SO_2 scrubbing. The economic NMPC problem was formulated to optimize the recycle spray flowrates with an ℓ_1 -penalty formulation to incorporate the SO_2 regulation constraint. The optimal control trajectory for the recycle flowrates indicated larger proportion of the recycle slurry being sent to the lowest spray header consistently in response to disturbances in the inlet flue gas flowrate.

Overall, the DAE model results in a well-posed, tractable simulation and optimization of the FGD unit. Moreover, several extensions and improvements on this model could be made so as to expand its features depending on the level of rigor desired. The model can be readily extended to include a larger number of species as discussed in Section 2. Additionally, metals that are typically involved in trace amounts could also be included. This would be advantageous if a more detailed study of the chemistry is to be conducted. The model could also be enhanced to investigate the influence of particle size distribution of limestone in the slurry and changing slurry droplet size along the tower. Establishment of a relationship between the reaction and absorption rates in the spray zone through an enhancement factor can provide useful insights that could be used to expand, and in some cases, simplify the FGD model. The economic NMPC problem could be improved to incorporate actual equipment costs in the objective function. Several other dynamic optimization and NMPC studies could also be investigated. With dynamic load disturbances, as well as transient plant conditions of ramp up and ramp down, it becomes difficult to maintain the quality of the byproduct gypsum. An NMPC framework could be built to maximize efficiency and

minimize deviations in the gypsum quality specifications under such conditions.

Disclaimer: This project was funded by the United States Department of Energy, National Energy Technology Laboratory, in part, through a site support contract. Neither the United States Government nor any agency thereof, nor any of their employees, nor the support contractor, nor any of their employees, makes any warranty, express or implied, or assumes any legal liability or responsibility for the accuracy, completeness, or usefulness of any information, apparatus, product, or process disclosed, or represents that its use would not infringe privately owned rights. Reference herein to any specific commercial product, process, or service by trade name, trademark, manufacturer, or otherwise does not necessarily constitute or imply its endorsement, recommendation, or favoring by the United States Government or any agency thereof. The views and opinions of authors expressed herein do not necessarily state or reflect those of the United States Government or any agency thereof.

Declaration of Competing Interest

The authors declare that they have no known competing financial interests or personal relationships that could have appeared to influence the work reported in this paper.

Acknowledgments

This work was conducted as part of the Institute for the Design of Advanced Energy Systems (IDAES) with support through the Simulation-Based Engineering, Crosscutting Research Program within the U.S. Department of Energy's Office of Fossil Energy and Carbon Management.

References

- Brogren, C., 1997. Models for wet scrubbing of SO_2 and NO_x (Ph.D.). Lund University.
- Brogren, C., Karlsson, H.T., 1997. Modeling the absorption of SO_2 in a spray scrubber using the penetration theory. *Chem. Eng. Sci.* 52 (18), 3085–3099.
- Chang, C.-S., Rochelle, G.T., 1981. SO_2 absorption into aqueous solutions. *AIChE J.* 27 (2), 292–298.
- Findeisen, R., Allgöwer, F., 2002. An introduction to nonlinear model predictive control. In: 21st Benelux meeting on systems and control, vol. 11. Technische Universiteit Eindhoven Veldhoven Eindhoven, The Netherlands, pp. 119–141.
- Gage, C.L., 1989. Limestone dissolution in modeling of slurry scrubbing for flue gas desulfurization (Ph.D. thesis). The University of Texas at Austin.
- Gage, C.L., Rochelle, G.T., 1992. Limestone dissolution in flue gas scrubbing: effect of sulfite. *J. Air Waste Manage. Assoc.* 42 (7), 926–935.
- Guo, Y., Xu, Z., Zheng, C., Shu, J., Dong, H., Zhang, Y., Weng, W., Gao, X., 2019. Modeling and optimization of wet flue gas desulfurization system based on a hybrid modeling method. *J. Air Waste Manage. Assoc.* 69 (5), 565–575.
- Hart, W.E., Watson, J.-P., Woodruff, D.L., 2011. Pyomo: modeling and solving mathematical programs in python. *Math. Program. Comput.* 3 (3), 219–260.
- Hart, W.E., Laird, C.D., Watson, J.-P., Woodruff, D.L., Hackebeil, G.A., Nicholson, B.L., Siirola, J.D., 2017. Pyomo—optimization modeling in python, second ed., vol. 67. Springer Science & Business Media.
- Huang, Y., Li, Y., Liu, X., Shen, J., 2017. Industrial application of constrained mpc with zone control to a coupled flue gas desulfurization system. In: 2017 Chinese Automation Congress (CAC). IEEE, pp. 2572–2578.
- Karatza, D., Prisciandaro, M., Lancia, A., Musmarra, D., 2005. Kinetic and reaction mechanisms of calcium bisulfite catalytic oxidation. *Chem. Eng. Sci.* 60 (6), 1497–1502.

- Kiil, S., Michelsen, M.L., Dam-Johansen, K., 1998. Experimental investigation and modeling of a wet flue gas desulfurization pilot plant. *Ind. Eng. Chem. Res.* 37 (7), 2792–2806.
- Kunkel, P., Mehrmann, V., 2004. Index reduction for differential-algebraic equations by minimal extension. *ZAMM J. Appl. Math. Mech./Zeitschrift für Angewandte Mathematik und Mechanik: Appl. Math. Mech.* 84(9), 579–597.
- Liu, P., Yang, L., Sun, L., 2021. Multi-objective economic model predictive control of wet limestone flue gas desulfurisation system. *Process Saf. Environ. Prot.* 150, 269–280.
- Lowell, P.S., Ottmers, D.M., Schwitzgebel, K., Strange, T.I., Deberry, D.W., 1970. A theoretical description of the limestone injection-wet scrubbing process. USEPAAPID 1287, PB 1931-029.
- Mattsson, S.E., Söderlind, G., 1993. Index reduction in differential-algebraic equations using dummy derivatives. *SIAM J. Sci. Comput.* 14 (3), 677–692.
- Naumann, Z., Schiller, L., 1935. A drag coefficient correlation. *Z. Ver. Deutsch. Ing* 77 (318), e323.
- Neveux, T., Le Moullec, Y., 2011. Wet industrial flue gas desulfurization unit: model development and validation on industrial data. *Ind. Eng. Chem. Res.* 50 (12), 7579–7592.
- Nygaard, H.G., Kiil, S., Johnsson, J.E., Jensen, J.N., Hansen, J., Fogh, F., Dam-Johansen, K., 2004. Full-scale measurements of SO₂ gas phase concentrations and slurry compositions in a wet flue gas desulphurisation spray absorber. *Fuel* 83 (9), 1151–1164.
- Pantelides, C.C., 1988. The consistent initialization of differential-algebraic systems. *SIAM J. Sci. Stat. Comput.* 9 (2), 213–231.
- Patwardhan, A.A., Rawlings, J.B., Edgar, T.F., 1990. Nonlinear model predictive control. *Chem. Eng. Commun.* 87 (1), 123–141.
- Petzold, L.R., 1982. Description of dassl: a differential/algebraic system solver. Tech. rep. Sandia National Labs., Livermore, CA (USA).
- Villanueva Perales, A., Ollero, P., Gutierrez Ortiz, F., Gómez-Barea, A., 2009. Model predictive control of a wet limestone flue gas desulfurization pilot plant. *Ind. Eng. Chem. Res.* 48 (11), 5399–5405.
- Wächter, A., Biegler, L.T., 2006. On the implementation of an interior-point filter line-search algorithm for large-scale nonlinear programming. *Math. Program.* 106 (1), 25–57.
- Wallin, M., Bjerle, I., 1989. A mass transfer model for limestone dissolution from a rotating cylinder. *Chem. Eng. Sci.* 44 (1), 61–67.
- Yang, X., Griffith, D.W., Biegler, L.T., 2015. Nonlinear programming properties for stable and robust nmpc. *IFAC-PapersOnLine* 48 (23), 388–397.
- Zhong, Y., Gao, X., Huo, W., Luo, Z.-Y., Ni, M.-J., Cen, K.-F., 2008. A model for performance optimization of wet flue gas desulfurization systems of power plants. *Fuel Process. Technol.* 89 (11), 1025–1032.